

# X-ray Hybrid CMOS Detectors: Recent Development and Characterization Progress

Tanmoy Chattopadhyay<sup>a</sup>, Abraham D. Falcone<sup>a</sup>, David N. Burrows<sup>a</sup>, Samuel Hull<sup>a</sup>, Evan Bray<sup>a</sup>, Mitchell Wages<sup>a</sup>, Maria Macquaide<sup>a</sup>, Lazar Buntic<sup>a</sup>, Ryan Crum<sup>a</sup>, Jessica O'Dell<sup>a</sup>, and Tyler Anderson<sup>a</sup>

<sup>a</sup>Pennsylvania State University, Department of Astronomy & Astrophysics, University Park, PA 16802, USA

## ABSTRACT

X-ray Hybrid CMOS Detectors (HCDs) have advantages over X-ray CCDs due to their higher readout rate abilities, flexible readout, inherent radiation hardness, and low power, which make them more suitable for the next generation large-area X-ray telescope missions. The Penn State high energy astronomy laboratory has been working on the development and characterization of HCDs in collaboration with Teledyne Imaging Sensors (TIS). A custom-made H2RG detector with 36  $\mu\text{m}$  pixel pitch and 18  $\mu\text{m}$  ROIC shows an improved performance over standard H1RG detectors, primarily due to a reduced level of inter-pixel capacitance crosstalk (IPC). However, the energy resolution and the noise of the detector and readout system are still limited when utilizing a SIDECAR at non-cryogenic temperatures. We characterized an H2RG detector with a Cryo-SIDECAR readout and controller, and we find an improved energy resolution of  $\sim 2.7\%$  at 5.9 keV and read noise of  $\sim 6.5\text{ e}^-$ . Detections of the  $\sim 0.525\text{ keV}$  Oxygen  $\text{K}\alpha$  and  $\sim 0.277\text{ keV}$  Carbon  $\text{K}\alpha$  lines with this detector display an improved sensitivity level at lower energies. This detector was successfully flown on NASA's first water recovery sounding rocket flight on April 4<sup>th</sup>, 2018. We have also been developing several new HCDs with potential applications for future X-ray astronomy missions. We are characterizing the performance of small-pixel HCDs (12.5  $\mu\text{m}$  pitch), which are important for the development of a next-generation high-resolution imager with HCDs. The latest results on these small pixel detectors has shown them to have the best read noise and energy resolution to-date for any X-ray HCD, with a measured 5.5  $\text{e}^-$  read noise for a detector with in-pixel correlated double sampling. Event recognition in HCDs is another exciting prospect. We characterized a  $64 \times 64$  pixel prototype Speedster-EXD detector that uses comparators in each pixel to read out only those pixels having detectable signal, thereby providing an order of magnitude improvement in the effective readout rate. Currently, we are working on the development of a large area Speedster-EXD with a  $550 \times 550$  pixel array. HCDs can also be utilized as a large FOV instrument to study the prompt and afterglow emissions of GRBs and detect black hole transients. In this context, we are characterizing a Lobster-HCD system for future CubeSat experiments. This paper briefly presents these new developments and experimental results.

**Keywords:** X-rays, X-ray Hybrid CMOS detector, SIDECAR, sounding rocket, proton irradiation

## 1. INTRODUCTION

X-ray Charge Coupled Devices (CCDs) [1, 2] have been the work-horse for soft X-ray instrumentation for more than two decades now, having been implemented in several X-ray astronomy missions, e.g., ASCA, Chandra, XMM-Newton, Swift, Integral, Hitomi, and AstroSat. These detectors provide moderate energy resolution, very low electronic read noise, and small pixel sizes that enable high angular resolution images of astronomical sources for Chandra-like X-ray mirrors. Existing missions have been extremely successful, and the next generation missions will build on that success by combining fine angular resolution and large collecting area in order to probe deeper into the high redshift and low luminosity universe [3]. Lynx (previously known as X-Ray Surveyor) [4],

---

Further author information: (Send correspondence to T. Chattopadhyay)  
T.C.: E-mail: txc344@psu.edu, Telephone: 1 814 852 9733

NASA’s 2020 decadal survey mission, for example, plans to have 30 times higher collecting area than Chandra. These upcoming missions, therefore, require focal plane detectors with faster readout speed than the existing modern-day X-ray CCDs, in order to avoid pile up and saturation effects in the detectors [5].

The new generation soft X-ray detectors should fulfill the following requirements imposed by upcoming large telescope missions (e.g. Lynx).

- The detectors should provide fast readout to avoid pile up effects.
- The detectors should provide nearly Fano-limited energy resolution with low electronic read noise for quality spectroscopic data.
- The pixel size should be small to provide high angular resolution images.
- The detectors should be radiation hard which is important for the detectors to operate longer and provide quality data over the years.

X-ray Hybrid CMOS detectors (hereafter X-ray HCDs) [6] are active pixel sensors and are expected to fulfill all of these requirements. The other advantage of these detectors is the low power requirement compared to CCDs (at least by a factor of 10). The Pennsylvania State University (PSU) has been collaborating with Teledyne Imaging Sensors (TIS) for more than a decade now on the technological development of X-ray HCDs and their characterization. PSU is involved in multiple activities and projects on X-ray HCDs to continue its technological development and improvement in the measurements for future astronomical missions [7].

In Sec. 1, we describe the main characteristics of X-ray HCDs followed up by recent improvement in energy resolution and read noise measurements for an H2RG detector with cryogenic SIDECAR in Sec. 3. The same H2RG detector is successfully launched in NASA’s first water recovery rocket experiment in early 2018. We will briefly describe the camera on this payload and the calibration of the instrument in Sec. 4. Sec. 5 briefly describes the new developments in X-ray HCDs, including both small-pixel detectors with in-pixel CDS and HCDs with event-driven readout and on-chip digitization, followed up by new experiments with X-ray HCDs to demonstrate their radiation hardness, sub-pixel localization capability, and wide field imaging capability.

## 2. X-RAY HYBRID CMOS DETECTORS (HCDS)

HCDs are active pixel sensors. For more than a decade now, PSU has been collaborating with TIS to develop X-ray HCDs based on TIS HAWAII series detectors [8]. X-ray HCDs are composed of two separate layers: one absorbing Silicon layer to absorb the photons and convert the deposited energy into charge, and the other Silicon layer is for the Readout Integrated Circuit (ROIC) to read out the charge of the individual pixels and convert them into voltage signal (see Fig. 1). The pixels in the Silicon layer are attached to the ROIC pixels by Indium bump bonds. Because of this kind of architecture of separate layers for absorption of photons and electronics, each layer can be optimized separately. For example, the absorbing layer can be made highly resistive so that the depletion depth can be as high as 500  $\mu\text{m}$  making these detectors sensitive to high energies  $> 20$  keV. On the other hand, the readout layer can also be optimized to accommodate new electronic components without affecting the Silicon absorbing layer.

HCDs provide several advantages over the modern day CCDs as described below.

- *Fast readout:* HCDs typically provide an order of magnitude faster readout speed compared to CCDs. The SIDECAR also facilitates parallel readout (4/16/32) channels with readout speeds of  $> 10$  Mpixel/s for each channel. High readout speed ensures the probability of pile up in the detector pixels to be extremely small, which is important in the context of large telescope area instruments. HCDs also provide readout in window mode where only a certain region of the detector plane will be readout. This feature is useful while observing bright transient events since this window can be made arbitrarily small in order to achieve huge sub-frame rates.

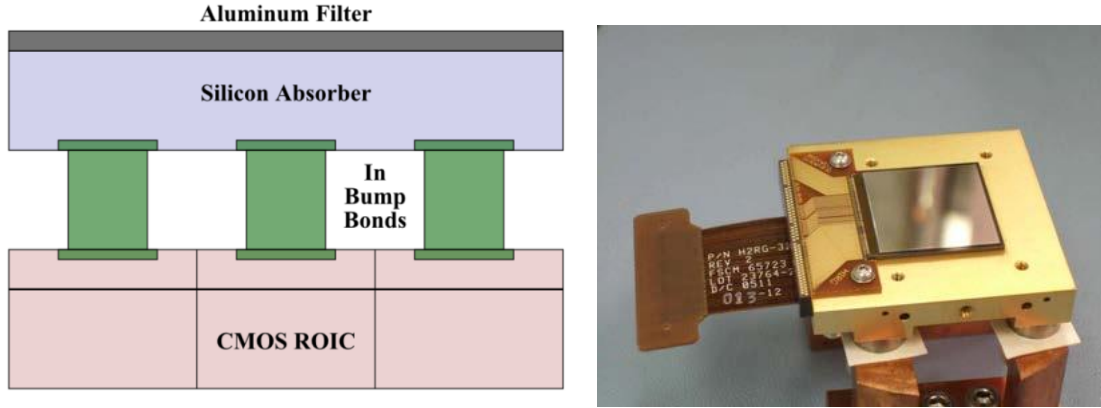


Figure 1. Left: Cross-sectional schematic of hybrid CMOS X-ray detector. Si absorbing layer is bump bonded to the read out electronics layer in each pixel, allowing for separate optimization. Right: Image of an HIRG hybrid CMOS detector ('1' stands for  $1024 \times 1024$  pixel array) with  $18 \mu\text{m}$  pixel pitch. There is a  $50 \text{ nm}$  Al layer deposited directly on the Si layer.

- *Radiation hardness:* CCDs are susceptible to proton displacement damage, and there are well known detector performance effects from radiation damage of the Chandra CCDs; e.g. [9]. Unlike transferring the charge across the pixels as in case of CCDs, HCDs readout the individual pixels. Therefore even if a HCD pixel is damaged, the whole column is not affected by that damage as is the case for CCDs.

Unlike CCDs, the gates of HCDs are not directly exposed, which makes HCDs less susceptible to micro-meteoroid damage [10].

- *Low power:* HCDs are low power devices. Amount of power consumed by an HCD is of the order of mW. For comparison, the CCD in XRT Swift [11] consumes  $\sim 8$  watts of power. An HCD can do all such operations for  $\sim 100 - 200$  mW of power. This is an important feature of HCDs which make them suitable for future X-ray astronomy missions.

### 3. CHARACTERIZATION OF HXRG DETECTORS

The first generation of the X-ray HCD devices delivered by TIS to PSU in 2006 were Hybrid Visible Silicon (HyViSi) detectors with HIRG ('1' stands for  $1024 \times 1024$  pixel array) CMOS ROIC in which we demonstrated the successful replacement of the normal anti-reflective coating (used for optical/IR detectors) with a  $500 \text{ nm}$  optical blocking filter directly deposited on the silicon detection layer [12]. A Teledyne SIDECAR \* is used to provide the clock and bias signals to the HxRGs. It also provides chip programming, signal amplification, analog-to-digital conversion, and data buffering. The SIDECAR is followed up by SIDECAR Acquisition Module (SAM) which provides further signal processing and amplification.

The modified HIRG detectors with  $18 \mu\text{m}$  pixel pitch (see Fig. 1) were characterized in detail using a PSU cube stand, which is a light tight vacuum chamber with pressure  $\sim 10^{-6}$  torr. The details of the experiment set up and the results have been reported in [7, 12, 13, 14, 15, 16]. The best energy resolution and read noise for HIRG detectors were found to be  $4.2 \%$  at  $5.9 \text{ keV}$  and  $16 \text{ e}^-$  respectively. The read noise and energy resolution are found to be limited by

1. Inter-pixel capacitance cross-talk (IPC) due to change in gate voltage while integrating the charge degrades the energy resolution. We experimentally estimated the IPC to be around  $10 \%$  of the signal shared with a given neighboring pixel.
2. There can be thermal voltage fluctuation in the SIDECAR ASIC during the integration of the charge. This effect can be reduced significantly by cooling the ASIC below  $200 \text{ K}$ .

\*<http://www.teledyne-si.com/ps-sidecar-asic.html>

3. Pixel to pixel gain variation also contribute to the read noise and energy resolution of the detector.

In order to reduce IPC (as described in [1]), a  $2048 \times 2048$  pixel H2RG readout integrated circuit (ROIC) was bump bonded to a  $36 \mu\text{m}$  pitch Silicon detector layer (with only a subset of the ROIC pixels bonded), such that the effective pixel size is  $36 \mu\text{m}$  instead of  $18 \mu\text{m}$ . This reduced the IPC significantly from 10 % to 1.8 % [15]. It is to be noted that in the modern X-ray HCD devices, implementation of capacitive transimpedance amplifier (CTIA) eliminates IPC, which will be discussed in later sections.

### 3.1 Characterization of an H2RG with cryogenic SIDECAR<sup>TM</sup>

In order to investigate the performance of the same H2RG detector with SIDECAR when cooled to cryogenic temperatures, we utilized a cryogenic SIDECAR ASIC from TIS. Cooling the ASIC to temperatures  $< 200 \text{ K}$ , with minimal thermal fluctuations, is expected to provide improved detector performance.

The experiment set up is shown in Fig. 2. The H2RG is directly mounted on the cold finger, whereas

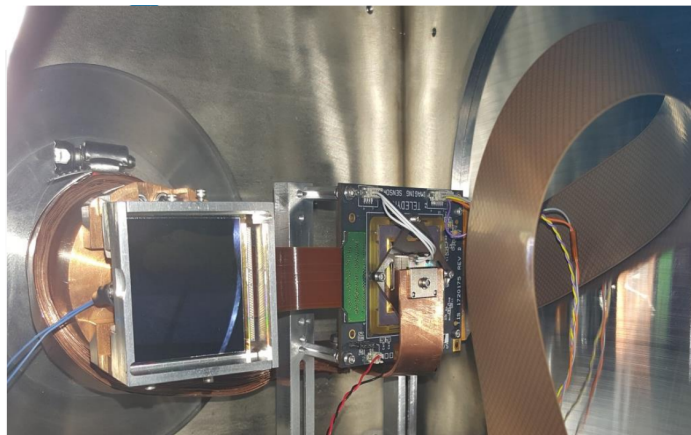


Figure 2. The interior of the test chamber with an H2RG hybrid CMOS detector attached to a cold finger and the cryogenic SIDECAR<sup>TM</sup> to the right of the detector, with a cold strap to cool the SIDECAR<sup>TM</sup>.

a cold strap is connected between the cold finger and the ASIC. The detector temperature is kept at 130 K using a Labview-controlled PID loop. The SIDECAR ASIC temperature was at 180 K. The detector was run in two different modes – 32 channel and 4 channel readout with frame times of 1.49 seconds and 10.65 seconds respectively. The raw images are processed using standard IDL-based routines where we first determine the channel to channel gain and offset variation and apply those corrections to CDS images. This is followed up by offset correction for each row in the image.

For characterization of the detector, we used an  $\text{Fe}^{55}$  radioactive source which emits 5.9 keV and 6.4 keV photons, as well as a  $\text{Po}^{210}$  source to induce fluorescence from targets that provided several low energy X-ray lines ranging from 0.525 keV (O  $\text{K}\alpha$ ) to 4.5 keV (Ti  $\text{K}\alpha$ ). We used single pixel events for the analysis. The spectra from these measurements are shown in Fig. 3. The Oxygen line is detected and well resolved, due partly to the improvement in the performance of the H2RG detector with the use of Cryo-SIDECAR operated at low temperature. It is to be noted that energy resolution of 2.7 % at 5.9 keV is the best ever energy resolution reported for an X-ray H2RG detector. We estimate the read noise to be  $\sim 6.5 \text{ e}^-$ .

## 4. X-RAY HCD IN WRX ROCKET PAYLOAD

The same H2RG detector with a Cryo-SIDECAR was recently flown in the Water Recovery X-ray (WRX) sounding rocket payload that was successfully launched from Kwajalein Atoll on April 4<sup>th</sup>, 2018. Notably, it was the first NASA astrophysics sounding rocket payload to attempt water recovery, and at the same time this is first time an X-ray HCD was flown in space. The payload consists of primary optics followed by off-plane reflection gratings [17], and a camera with the H2RG detector along with the cryo-SIDECAR and a custom

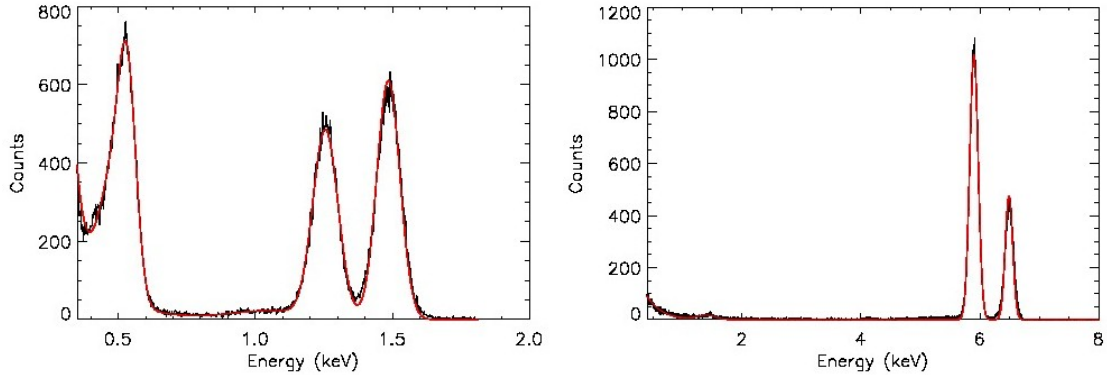


Figure 3. Left: An H2RG spectrum of O  $K\alpha$  (0.525 keV), Mg  $K\alpha$  (1.25 keV), and Al  $K\alpha$  (1.49 keV) lines. A fit to the data is shown in red. Right: Same for Mn  $K\alpha$  and  $K\beta$  lines at 5.9 keV and 6.4 keV.

camera interface board. A wide field of view ( $3.25^\circ \times 3.25^\circ$ ) enabled observations of a large region of the Vela supernova remnant, with a science goal to observe 3rd and 4th order OXII. Key technology goals were the technology demonstration in a space environment of X-ray hybrid CMOS detectors, and the demonstration of the water recovery techniques and technology. The technology readiness level (TRL) of X-ray HCDs was successfully raised to TRL 9. Analysis of the flight data is currently under progress and will be reported elsewhere. In this section, we briefly describe the instrument and the ground calibration of the payload.

The spectrometer design consists of a mechanical collimator, X-ray reflection gratings, a mirror module, and the hybrid CMOS detector camera. X-rays entering through the lightweight wire-grid collimator are intercepted by the off-plane reflection gratings and dispersed to produce spectral lines on the detector plane with  $\sim 190$  mm cross-dispersion extent. Because the size of the H2RG detector is  $35 \text{ mm} \times 35 \text{ mm}$ , this would result in less than 20 % of a given spectral line falling on the detector area. To mitigate this large line dispersion, a mirror module is inserted between the reflection gratings and the camera. This module contains an array of nickel-coated mirrors that reflect light back onto the detector area to minimize photon losses from the gratings. For a more complete description of the instrument design and full specifications, see [18].

The camera package is a custom built  $8.5 \times 8.5 \times 12.75$  inch enclosure that is mounted at the spectrometer focal plane (see Fig. 4 (left)). Inside, a copper cold finger cools the H2RG and the cryogenic SIDECAR to 130 K and 175 K respectively. This temperature was cold-biased to a temperature that is much lower than required since the camera was expected to warm up during launch and flight, after the liquid nitrogen was pulled away. Because this particular H2RG detector does not have an aluminum filter deposited directly onto it, a 45 nm Ti plus 70 nm Al filter was procured from Luxel and installed in front of the detector surface. A  $\text{Fe}^{55}$  calibration source was mounted inside the enclosure to enable valuable in-flight calibration X-rays (seen above the filter in Fig. 4). The detector housing was isolated from the main instrument vacuum section by a controllable GN2 actuated gate valve, protecting the detector from external factors when not pointed at the science target; an on-board ion pump was used to maintain the vacuum pressure in the enclosure. At PSU, we developed a Camera Interface Board (CIB) which interacts with the SIDECAR ASIC to provide power, filtering, and data buffering (shown in the right panel in Fig. 4). The successful use of this CIB board in space also raises the CIB to TRL-9. The detector was run with 32 parallel output channels, providing a frame time of 1.48 seconds. A 15 V bias voltage was applied to the H2RG substrate.

Ground calibrations of the payload were done in two steps. In the first step, we calibrated the camera package i.e. the H2RG detector, Cryo SIDECAR, and the CIB. In the second step, we did end-to-end calibration of the complete payload, i.e. the camera package, grating module, mirror module with the flight electronics inside the rocket experiment section. The detector was planned to be initially cooled to 130 K, and during the flight, the temperature would drift up from 130 K. Therefore, we calibrated the camera package at multiple temperatures (from 125 K – 170 K) and at multiple line energies (0.525 keV – 6.4 keV). Data were collected in 32 channel and processed by the same IDL pipeline for cleaning, event grading based on Swift XRT grading scheme [11],

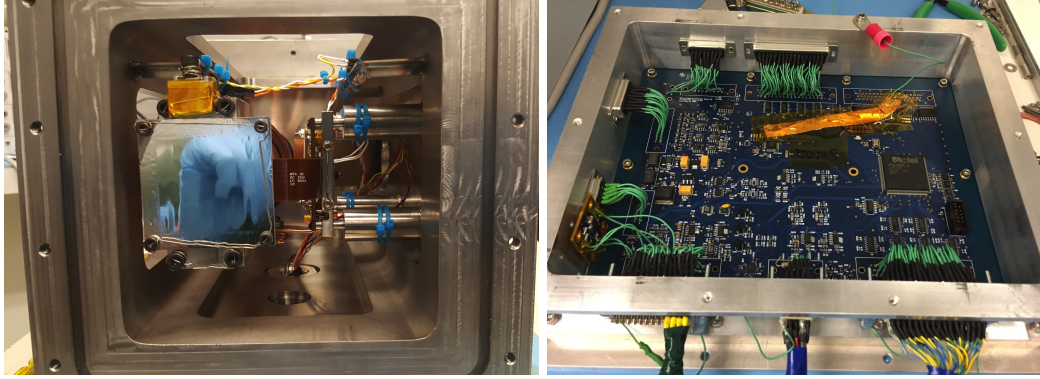


Figure 4. Left: Picture of the interior of the camera chamber. The H2RG detector is mounted on the cold finger. The reflection of the blue glove can be seen on the optical filter. The cryo-SIDECAR to the right of the detector is mounted on the side wall using four standoffs. There is a  $\text{Fe}^{55}$  calibration source at the top left corner of the filter. Right: Image of the Camera Interface Board (CIB) developed at PSU. The CIB interfaces the Cryo-SIDECAR and the spacecraft. The CIB is attached to the back wall of the chamber.

and finally to generate the spectra. The top-left plot in Fig. 5 shows the linearity of the detector at multiple temperatures for O  $K\alpha$  (0.525 keV), Mg  $K\alpha$  (1.25 keV), Al  $K\alpha$  (1.49 keV), Mn  $K\alpha$  (5.9 keV) and Mn  $K\beta$  (6.4 keV) lines. We estimated the gain and offset for each of these temperatures. The top-right plot in Fig. 5 shows

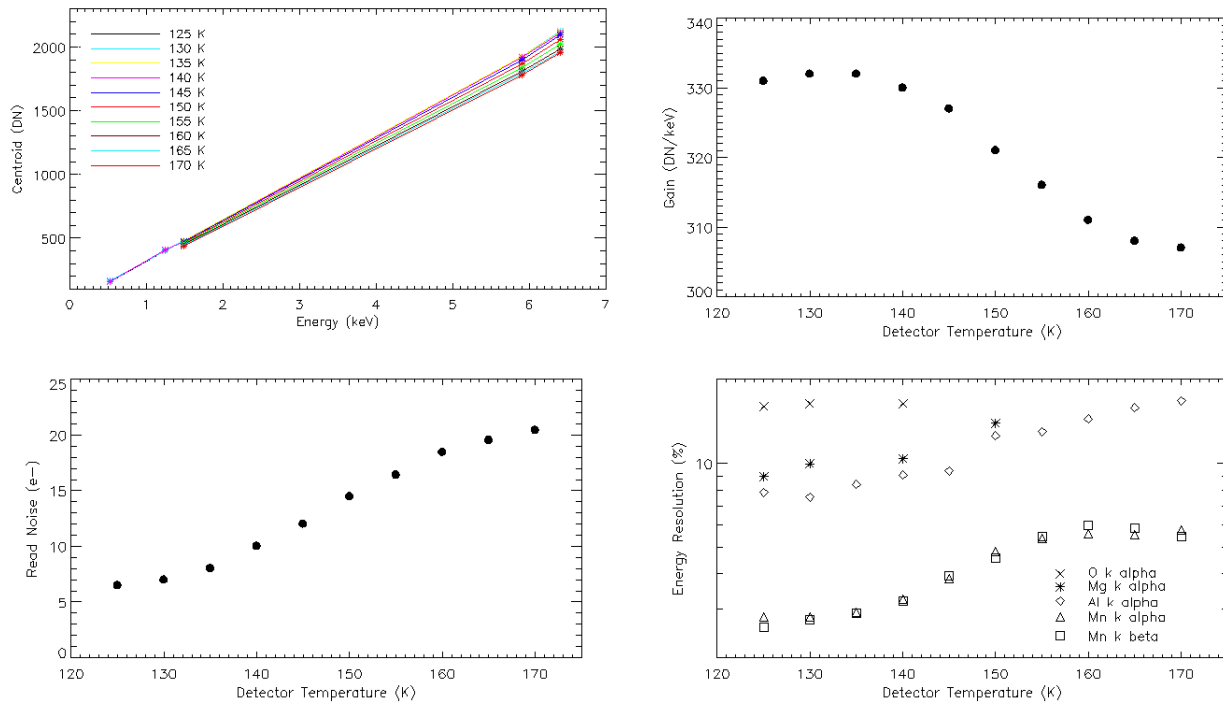


Figure 5. Top-left: Linearity of the detector in the energy range of 0.525 – 6.4 keV at multiple temperatures from 125 K to 170 K. Top-right: The gain of the detector as a function of temperature. Bottom-left: Dependence of read noise of the camera on temperature. Bottom-right: Change in energy resolution of the camera with temperature for O  $K\alpha$  (0.525 keV), Mg  $K\alpha$  (1.25 keV), Al  $K\alpha$  (1.49 keV), Mn  $K\alpha$  (5.9 keV) and Mn  $K\beta$  (6.4 keV).

the variation of gain as function of temperature. Knowledge of variation of gain with temperature is important in order to correct the flight data for the drift in temperature. The bottom-left plot shows the read noise of the

camera as a function of temperature. At 125 K, the read noise is around 6.5  $e^-$  and increases steadily till 160 K and then starts leveling out. Dependence of energy resolution on the temperature for different energy lines is shown in the bottom-right plot. From these results, it is evident that there is no significant change in gain, resolution and read noise in 125 K – 135 K region. At temperatures beyond 150 K for the detector and 185 K for the SIDE CAR, the detector noise and energy resolution begin to increase. All of these measurements were repeated multiple times.

In the second step, we calibrated the camera package inside the rocket experiment section with the grating module and the mirror module as shown in Fig. 6. A Manson X-ray source was used to generate X-rays from

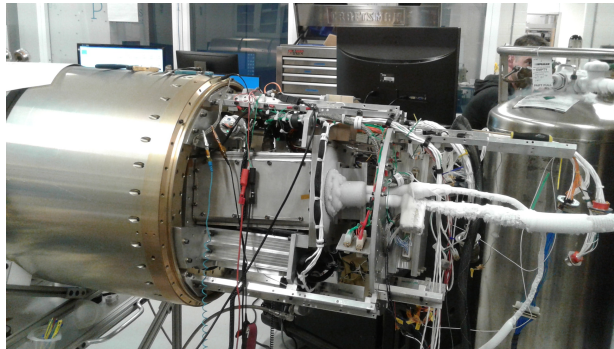


Figure 6. End-to-end calibration of the rocket payload. The grating and the mirror module is inside the rocket chamber. The camera package chamber can be seen in the picture. The liquid Nitrogen ( $LN_2$ ) cylinder (shown in the image) supplies  $LN_2$  to cool down the detector and the Cryo-SIDE CAR during calibration. An X-ray source (Manson source) is connected to the other end of the rocket chamber to generate X-rays.

the other end of the rocket section. The Manson source uses a number of target anodes (Carbon, Magnesium, Aluminum, Copper etc.) where electrons from hot filament are accelerated towards the target by a strong electric field. The electrons generate bremsstrahlung radiation plus the  $K\alpha$  lines from the anodes. Fig 7 (top) shows the histogram of events in the detector plane with different colors indicating number of events per pixel. The grating module disperse the spectral lines in different regions in the detector plane. Three different lines are clearly visible in the image where the line at the top region corresponds to Carbon  $K\alpha$  line, the middle region corresponds to Oxygen  $K\alpha$  and the region at the bottom corresponds to Nitrogen  $K\alpha$  line. The spectra obtained from these regions are shown in the bottom panel of the figure.

## 5. RECENT DEVELOPMENTS IN X-RAY HCDs

### 5.1 Small Pixel HCDs

The small pixel HCDs are new prototype HCDs developed in collaboration between PSU and TIS. The detectors were designed to satisfy the requirements of future fine angular resolution X-ray missions (e.g. Lynx): small pixel size, fast readout, and  $< 4 e^-$  read noise. The  $128 \times 128$  prototype arrays have  $12.5 \mu m$  pixel pitch with  $100 \mu m$  fully depleted depth. The detectors use CTIA amplifier in each pixel, which unlike the source follower amplifier in the HAWAII HCDs, holds the gate voltage constant during integration and eliminates inter-pixel capacitive crosstalk. The arrays also have the capability to perform in-pixel correlated double sampling (CDS) by subtracting the variable baseline voltage associated with a reset and thus remove reset KTC noise. Fig. 8 (left) shows the picture of an engineering grade small pixel HCD test device.

Recent work has involved characterization of the small pixel detectors, including estimation of the pixel-to-pixel gain variation. The gain variation was calculated to be  $\sim 1.1\%$ , and gain corrected energy spectra were obtained. Fig. 8 (right) shows the Mn  $K\alpha$  and Mn  $K\beta$  spectrum after correcting for the gain variation — the measured energy resolution at 5.9 keV is  $\sim 150 eV$  ( $\sim 2.7\%$ ) — while the read noise is measured to be as low as  $5.54 e^-$ . These are the best ever energy resolution and read noise measurements for any X-ray HCD detector reported to-date. Details of the experiment and these characterizations can be found in [19]. Currently, we are

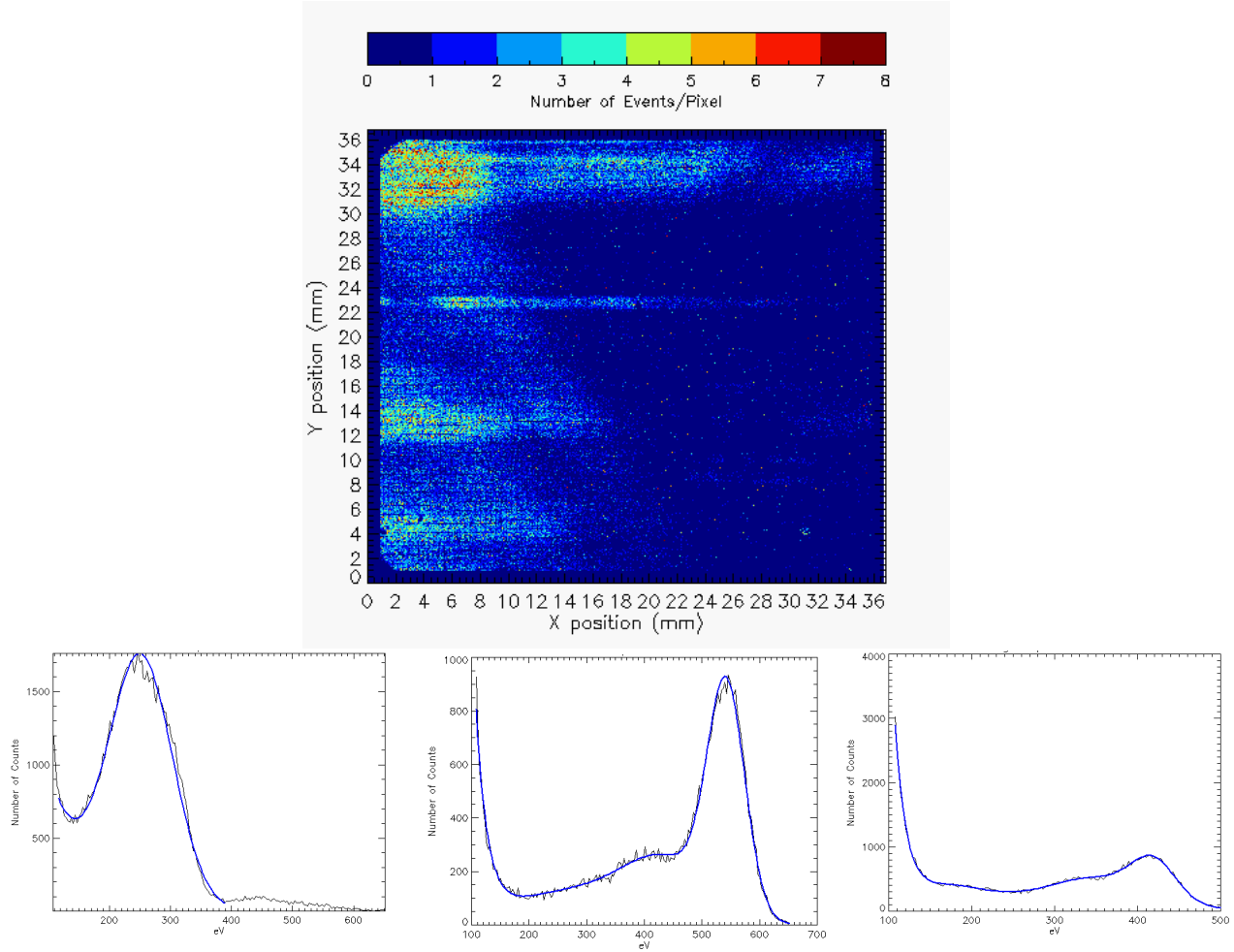


Figure 7. Top: 2D histogram of the X-ray events in the detector plane. The number of events per pixel is shown in colors. The grating module dispersed the X-ray photons of different energies to different regions of the detector where the top, middle and the bottom regions correspond to C  $K\alpha$  (0.27 keV), O  $K\alpha$  (0.525 keV), N  $K\alpha$  (0.39 keV) respectively. Bottom (left to right): The corresponding spectra of C  $K\alpha$  (0.27 keV), O  $K\alpha$  (0.525 keV), and N  $K\alpha$  (0.39 keV) lines. The blue solid lines are the fit to the spectra.

scaling this test design up to a large format detector with on-chip digitization, while attempting to further reduce read noise through improved component tolerances.

## 5.2 Speedster-EXD

The Speedster-EXD is an advanced design utilizing a CTIA, in-pixel CDS, and event recognition circuitry to provide event-driven sparse readout. Event-driven readout is accomplished using a comparator that samples the CDS output and triggers on X-ray events. This provides timing resolution improvements by several orders of magnitude and a significant improvement in high count-rate applications. Fig. 9 shows an image of a Speedster detector with  $64 \times 64$  pixel array with  $40 \mu\text{m}$  pixel size and  $100 \mu\text{m}$  depletion depth. Fig. 10 shows the comparison of full frame readout mode (where the comparator threshold is set below the noise floor) and sparse readout mode (comparator threshold  $>$  noise floor). In the sparse readout mode, the  $3 \times 3$  region of pixels surrounding the pixels above comparator threshold is read out. The Speedster-EXD prototype devices have been characterized in terms of read noise, energy resolution, IPC, dark current, pixel-to-pixel gain variation. Energy resolution was found to be around 3.5 % at 5.9 keV. IPC was found to be negligible. More details on the experiment set-up and characterization can be found in [20]. A larger version of Speedster detectors is currently



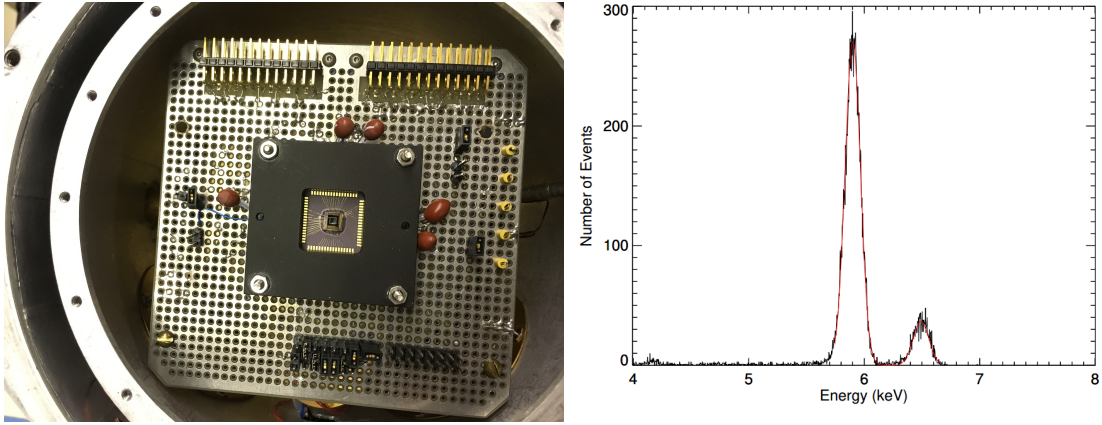


Figure 8. Left: Small pixel FPA 18567 seated in breadboard inside testing dewar. The breadboard measures  $10\text{ cm} \times 10\text{ cm}$ . Right: Gain corrected  $\text{Fe}^{55}$  X-ray spectra for FPA 18568, showing the Mn  $K\alpha$  and Mn  $K\beta$  lines at 5.9 keV and 6.4 keV. See text for details.

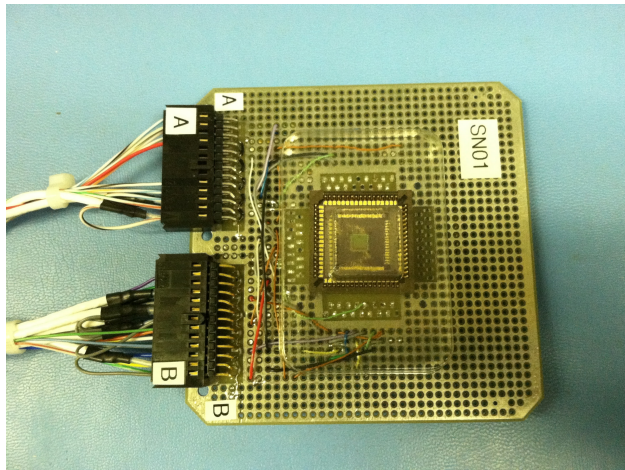


Figure 9. Photo of a prototype of Speedster-EXD detector. There are total  $64 \times 64$  pixels with  $40\ \mu\text{m}$  pixel size. To block the optical light, there is a 50 nm Al layer directly deposited on the Si layer.

being developed. The new detectors will be  $2.2\text{ cm} \times 2.2\text{ cm}$  in size, with  $550 \times 550$  pixel array ( $40\ \mu\text{m}$  pixel size). The input cell architecture also supports multiple readout nodes in order to maintain the high readout speed. The detectors also include on-chip analog-to-digital conversion.

## 6. OTHER ONGOING ACTIVITIES WITH HCDS

### 6.1 Sub-pixel resolution in HCDS

It is possible to exploit the charge sharing effect in pixelated detectors to find the exact location of the incident X-ray photons, which in turn can increase the scientific yield of a single observation by overcoming limitations of pixel size by more thoroughly sampling the PSF of X-ray telescopes. Recently, we performed a “mesh experiment” to experimentally determine the charge cloud shape for a custom H2RG with  $36\ \mu\text{m}$  pixels at 1.5 keV. For more details, refer to [21]. Once the charge cloud shape is known, X-ray landing location can be determined with subpixel resolution. We found that X-ray landing location can be accurately determined in directions that exhibit charge sharing between pixels. For a 2-pixel event, the positional resolution can be obtained with an accuracy of  $\sim 0.5\ \mu\text{m}$  in the direction of charge split and  $\sim 7\ \mu\text{m}$  in the other direction at 68% confidence level. For a 3-pixel event, the position resolution improves to  $\sim 0.5\ \mu\text{m}$  (68% confidence) in both directions.

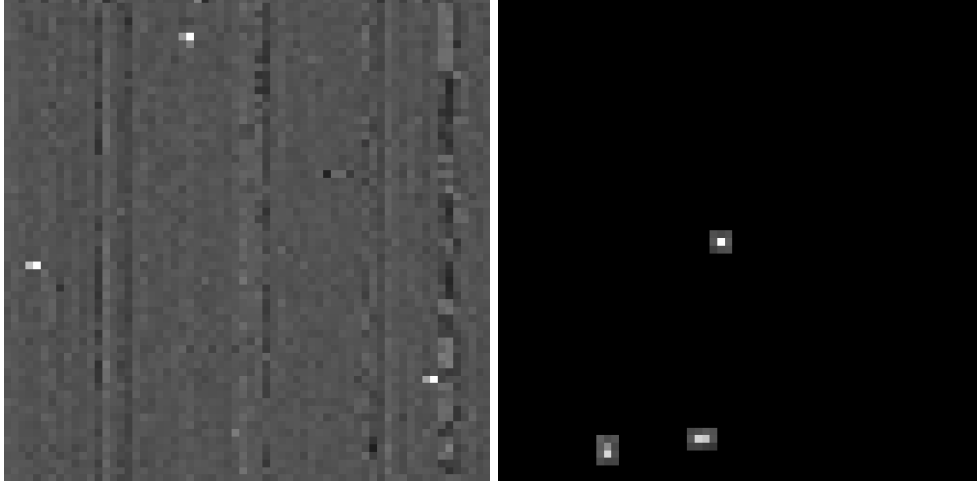


Figure 10. Left: Full Frame Readout Mode. The comparator is set below the noise floor and thus every pixel in the array is read out. Three multi-pixel  $\text{Fe}^{55}$  events can be seen, in addition to all background pixels. Right :  $3 \times 3$  Sparse Readout Mode. The comparator is set above the noise floor, allowing read out of only X-ray events and their neighboring pixels. Two multi-pixel and one single pixel  $\text{Fe}^{55}$  X-ray events can be seen, with their  $3 \times 3$  regions.

Based on these experimental results, we have developed a model to predict the charge sharing and subpixel resolution as a function of X-ray landing position and applied it to a prototype  $12.5 \mu\text{m}$  pitch small-pixel HCD that would be suitable for the Lynx X-ray surveyor [22]. When operated with a substrate voltage of 80V, we determined a spatial resolution of  $0.2 - 1.2 \mu\text{m}$  (68% confidence) for all events. When operated at 15V, the charge cloud becomes significantly larger, and we determine a spatial resolution of  $0.4 - 0.6 \mu\text{m}$  (68% confidence) for all events. A summary of subpixel resolution results is shown in Table 1.

	68% Confidence region half-width ( $\mu\text{m}$ )					
	H2RG		Small pixel HCD ( $V_{\text{sub}}=80\text{V}$ )		Small pixel HCD ( $V_{\text{sub}}=15\text{V}$ )	
	$36 \mu\text{m}$		$12.5 \mu\text{m}$		$12.5 \mu\text{m}$	
<b>Pixel Pitch:</b>	x	y	x	y	x	y
<b>X-ray landing location within pixel</b>						
Center	7.1	7.1	1.2	1.2	0.6	0.6
Right	0.4	7.1	0.2	1.2	0.4	0.4
Bottom	7.1	0.4	1.2	0.2	0.4	0.4
Bottom-right	0.4	0.4	0.2	0.2	0.4	0.4

Table 1. A quantitative summary of the subpixel resolutions that can be achieved with the H2RG and small pixel HCD. X-ray landing location can be constrained very well in directions that exhibit charge sharing with neighboring pixels.

## 6.2 Radiation hardness of HCDs

Due to the short distance that collected charge must be transferred through the detector, HCDs are inherently radiation hard relative to CCDs. Once in orbit, the primary cause of performance degradation is displacement damage caused by high energy protons trapped in the radiation belts. In order to investigate the effect of irradiation in HCDs, we irradiated an HIRG HCD with 8 MeV protons, up to a total dose of 3 krad(Si) ( $4.5 \times 10^9$  protons/cm<sup>2</sup>) [23]. The experiment was conducted at the Edwards Accelerator Lab, which is operated by the Physics Department at Ohio University. After irradiation, we performed detailed characterization of the detector to investigate the effects of irradiation on read noise, dark current, gain, and energy resolution. After 3 months, detector characteristics appear to be returning to the pre-irradiation level. We plan to continue this collaboration in the coming months by returning to Ohio University to carry out further irradiations of higher doses.

### 6.3 Wide field imaging with HCDs

We are exploring the possibility to utilize HCD detectors as a wide field imager to study GRBs and X-ray black hole transients for future CubeSat missions. The low power requirement of the HCDs and their fast readout make them suitable for the study of transients in CubeSat missions. In this context, we have initiated characterization of an HIRG detector and a 2D Schmidt Lobster optic [24] in collaboration with Czech Republic Technical University (CTU). We utilize the 50 meter beam line at PSU to characterize the mirror at multiple energies and multiple off-axis angles. The optic FOV is  $5^\circ \times 5^\circ$  and 30 cm focal length (See [25] for more details). The left plot in Fig. 11 shows the obtained Point Spread Function (PSF) of the Lobster at 1.5 keV. The angular

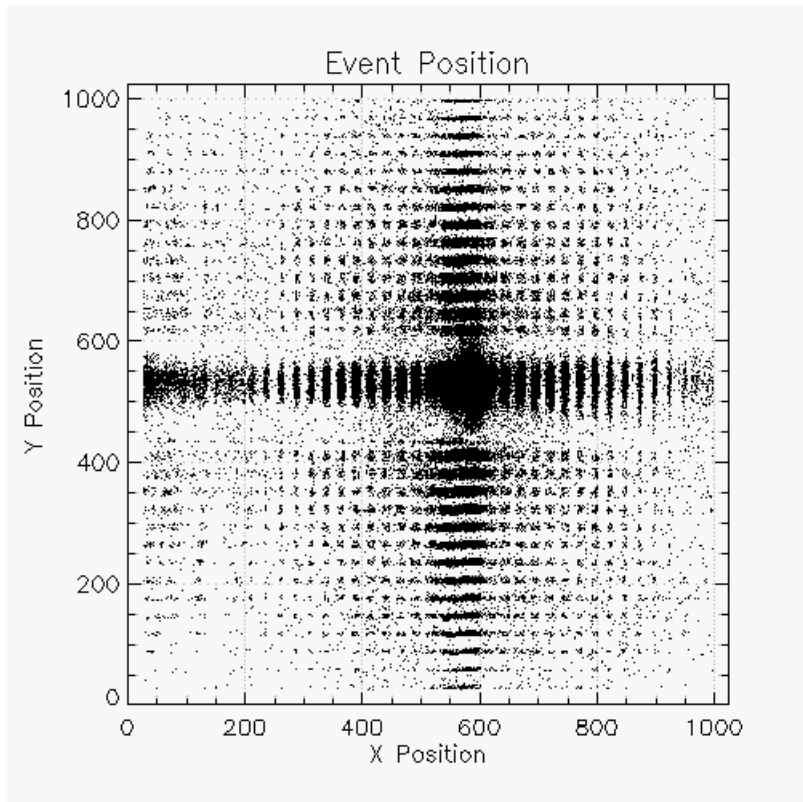


Figure 11. Point Spread Function (PSF) of the 2D lobster at 1.49 keV. The angular resolution is estimated to be  $\sim 6$  arc-min.

resolution is found to be  $\sim 6$  arc-min. The details of the experiment set up and results will be reported elsewhere.

Recently, we submitted a 6U class CubeSat proposal to NASA for a wide field imaging instrument consisting of an array of X-ray hybrid CMOS detectors at the focal plane of a coded aperture mask (BlackCAT; the Black hole Coded Aperture Telescope). The FOV of the instrument is  $\sim 60^\circ \times 60^\circ$  and sensitive in 0.5 – 20 keV. The primary science goals of the mission are to detect and locate high redshift GRBs and the electro-magnetic counterparts to the gravity waves with sub-arcmin accuracy, while monitoring the X-ray sky to detect and study black hole transients. For more details, on the conceptual design of the instrument and science goals, see [26].

## 7. SUMMARY

The PSU X-ray detector lab is involved in various activities relating to hybrid CMOS detectors and their continued technological development. We demonstrated significant improvement in energy resolution and read noise for an H2RG when the SIDECAR ASIC is cooled down below 180 K. The same H2RG detector and the cryo-SIDECAR was flown successfully in NASA's first Water Recovery X-ray Rocket flight on April 4<sup>th</sup>, 2018

from Kwajalein Atoll. The success of the mission raised the TRL of X-ray hybrid CMOS detectors to TRL-9, demonstrating their suitability for future space missions. The TRL of the Camera Interface Board (CIB) which was developed at PSU to interface the SIDECAR and the spacecraft has also been raised to TRL-9. Small pixel HCDs with  $12.5\ \mu\text{m}$  pixel pitch, in-pixel CDS, and CTIA amplifiers have also been characterized, with  $\sim 5.5$  e-read noise measured. After measuring the pixel-to-pixel gain variation, the resultant spectra for the small pixel HCDs provides energy resolution of  $\sim 2.7\%$  at 5.9 keV, which is very close to the Fano limit and is the best ever reported for X-ray hybrid CMOS detectors. Speedster-EXD prototypes are shown to improve the readout speed of HCDs by a several orders of magnitude and currently PSU and TIS are working on the development of a large array Speedster-EXD device. By performing a mesh experiment, we also demonstrated the feasibility of achieving sub-pixel resolution with HCDs. Other efforts in our lab include investigation of proton irradiation effects on HCDs, thereby demonstrating the radiation hardness of HCDs. We are also planning to utilize X-ray HCDs as a wide field imager for future CubeSat missions to detect and study gravity wave event counterparts, high redshift GRBs, and black hole transients.

## ACKNOWLEDGMENTS

We gratefully acknowledge Teledyne Imaging Sensors, particularly Vincent Douence, Mihail Milkov, Steven Chen, Mark Farris, and Yibin Bai for their very useful troubleshooting assistance and their excellent design work. This work was supported by NASA grants NNX13AE57G, NNX17AE35G, NNX14AH68G, NNX17AD87G, NNX16AE27G, and 80NSSC18K0147.

## References

- [1] Lesser, M., “A summary of charge-coupled devices for astronomy,” *Publications of the Astronomical Society of the Pacific* **127**(957), 1097 (2015).
- [2] Gruner, S. M., Tate, M. W., and Eikenberry, E. F., “Charge-coupled device area x-ray detectors,” *Review of Scientific Instruments* **73**(8), 2815–2842 (2002).
- [3] Vikhlinin, A., Reid, P., Tananbaum, H., Schwartz, D. A., Forman, W. R., Jones, C., Bookbinder, J., Cotroneo, V., Trolrier-McKinstry, S., Burrows, D., Bautz, M. W., Heilmann, R., Davis, J., Bandler, S. R., Weisskopf, M. C., and Murray, S. S., “SMART-X: Square Meter Arcsecond Resolution x-ray Telescope,” in [*Space Telescopes and Instrumentation 2012: Ultraviolet to Gamma Ray*], *Society of Photo-Optical Instrumentation Engineers (SPIE) Conference Series* **8443**, 844316 (Sept. 2012).
- [4] Gaskin, J. A., Weisskopf, M. C., Vikhlinin, A., Tananbaum, H. D., Bandler, S. R., Bautz, M. W., Burrows, D. N., Falcone, A. D., Harrison, F. A., Heilmann, R. K., Heinz, S., Hopkins, R. C., Kilbourne, C. A., Kouveliotou, C., Kraft, R. P., Kravtsov, A. V., McEntaffer, R. L., Natarajan, P., O’Dell, S. L., Petre, R., Prieskorn, Z. R., Ptak, A. F., Ramsey, B. D., Reid, P. B., Schnell, A. R., Schwartz, D. A., and Townsley, L. K., “The X-ray Surveyor Mission: a concept study,” in [*UV, X-Ray, and Gamma-Ray Space Instrumentation for Astronomy XIX*], *Society of Photo-Optical Instrumentation Engineers (SPIE) Conference Series* **9601**, 96010J (Aug. 2015).
- [5] Lumb, D. H., “Simulations and Mitigation of Pile-Up in XMM CCD Instruments,” *Experimental Astronomy* **10**, 439–456 (Nov. 2000).
- [6] Bai, Y., Bajaj, J., Beletic, J. W., Farris, M. C., Joshi, A., Lauxtermann, S., Petersen, A., and Williams, G., “Teledyne Imaging Sensors: Silicon CMOS imaging technologies for x-ray, UV, visible, and near infrared,” **7021**, 702102 (July 2008).
- [7] Hull, S. V., Falcone, A. D., Burrows, D. N., Wages, M., Chattopadhyay, T., McQuaide, M., Bray, E., and Kern, M., “Recent X-ray hybrid CMOS detector developments and measurements,” **10397**, 1039704 (Aug. 2017).

- [8] Loose, M., Farris, M. C., Garnett, J. D., Hall, D. N. B., and Kozlowski, L. J., “HAWAII-2RG: a 2k x 2k CMOS multiplexer for low and high background astronomy applications,” in [*IR Space Telescopes and Instruments*], Mather, J. C., ed., *Society of Photo-Optical Instrumentation Engineers (SPIE) Conference Series* **4850**, 867–879 (Mar. 2003).
- [9] Grant, C. E., Bautz, M. W., Kissel, S. M., LaMarr, B., and Prigozhin, G. Y., “Long-term trends in radiation damage of Chandra x-ray CCDs,” in [*UV, X-Ray, and Gamma-Ray Space Instrumentation for Astronomy XIV*], Siegmund, O. H. W., ed., *Society of Photo-Optical Instrumentation Engineers (SPIE) Conference Series* **5898**, 201–211 (Aug. 2005).
- [10] Strüder, L., Aschenbach, B., Bräuninger, H., Drolshagen, G., Englhauser, J., Hartmann, R., Hartner, G., Holl, P., Kemmer, J., Meidinger, N., Stübig, M., and Trümper, J., “Evidence for micrometeoroid damage in the pn-CCD camera system aboard XMM-Newton,” *Astronomy and Astrophysics* **375**, L5–L8 (Aug. 2001).
- [11] Burrows, D. N., Hill, J. E., Nousek, J. A., Kennea, J. A., Wells, A., Osborne, J. P., Abbey, A. F., Beardmore, A., Mukerjee, K., Short, A. D. T., Chincarini, G., Campana, S., Citterio, O., Moretti, A., Pagani, C., Tagliaferri, G., Giommi, P., Capalbi, M., Tamburelli, F., Angelini, L., Cusumano, G., Bräuninger, H. W., Burkert, W., and Hartner, G. D., “The Swift X-Ray Telescope,” *Space Science Review* **120**, 165–195 (Oct. 2005).
- [12] Falcone, A. D., Burrows, D. N., Bai, Y., Farris, M., Cook, R., and Bongiorno, S., “Hybrid CMOS x-ray detectors: the next generation for focused x-ray telescopes,” *SPIE: UV, X-Ray, and Gamma-Ray Space Instrumentation for Astronomy XV* **6686**, 668602 (Sept. 2007).
- [13] Falcone, A. D., Prieskorn, Z., Griffith, C., Bongiorno, S., and Burrows, D. N., “Recent progress on developments and characterization of hybrid CMOS x-ray detectors,” *SPIE: High Energy, Optical, and Infrared Detectors for Astronomy V* **8453**, 84530E (July 2012).
- [14] Bongiorno, S. D., Falcone, A. D., Burrows, D. N., Cook, R., Bai, Y., and Farris, M., “Measurements of Si hybrid CMOS x-ray detector characteristics,” **7435**, 74350E (Aug. 2009).
- [15] Prieskorn, Z., Griffith, C. V., Bongiorno, S. D., Falcone, A. D., and Burrows, D. N., “Characterization of Si hybrid CMOS detectors for use in the soft X-ray band,” *Nuclear Instruments and Methods in Physics Research A* **717**, 83–93 (July 2013).
- [16] Prieskorn, Z. R., Bongiorno, S. D., Burrows, D. N., Falcone, A. D., Griffith, C. V., and Nikoleyczik, J., “Soft x-ray quantum efficiency of silicon hybrid CMOS detectors,” in [*High Energy, Optical, and Infrared Detectors for Astronomy VI*], *Society of Photo-Optical Instrumentation Engineers (SPIE) Conference Series* **9154**, 915410 (July 2014).
- [17] McEntaffer, R., DeRoo, C., Schultz, T., Gantner, B., Tutt, J., Holland, A., O’Dell, S., Gaskin, J., Kolodziejczak, J., Zhang, W. W., Chan, K.-W., Biskach, M., McClelland, R., Iazikov, D., Wang, X., and Koecher, L., “First results from a next-generation off-plane X-ray diffraction grating,” *Experimental Astronomy* **36**, 389–405 (Aug. 2013).
- [18] Miles, D. M., McEntaffer, R. L., Schultz, T. B., Donovan, B. D., Tutt, J. H., Yastishock, D., Steiner, T., Hillman, C. R., McCoy, J. A., Wages, M., Hull, S., Falcone, A., Burrows, D. N., Chattopadhyay, T., Anderson, T., and McQuaide, M., “An introduction to the water recovery x-ray rocket,” in [*Society of Photo-Optical Instrumentation Engineers (SPIE) Conference Series*], *Society of Photo-Optical Instrumentation Engineers (SPIE) Conference Series* **10397**, 103970R (Aug. 2017).
- [19] Hull, S. V., Falcone, A. D., Burrows, D. N., Wages, M., and McQuaide, M., “Small pixel hybrid cmos detectors,” in [*Space Telescopes and Instrumentation 2018: Ultraviolet to Gamma Ray*], *Proc.SPIE* **10709** (2018).
- [20] Griffith, C. V., Falcone, A. D., Prieskorn, Z. R., and Burrows, D. N., “The Speedster-EXD- A New Event-Driven Hybrid CMOS X-ray Detector,” *Journal of Astronomical Telescopes, Instruments, and Systems* **2**, 016001 (Jan. 2016).

- [21] Bray, E., Falcone, A. D., Chattopadhyay, T., Wages, M., and Burrows, D. N., “Characterizing subpixel spatial resolution of a hybrid cmos detector,” *Submitted to JATIS* .
- [22] Bray, E., Falcone, A. D., Hull, S. V., and Burrows, D. N., “Exploring fine subpixel spatial resolution of hybrid cmos detectors,” in [*Space Telescopes and Instrumentation 2018: Ultraviolet to Gamma Ray*], *Proc.SPIE* **10699** (2018).
- [23] Bray, E., Falcone, A. D., Wages, M., and Burrows, D. N., “Proton radiation damage experiment on a hybrid cmos detector,” in [*High Energy, Optical, and Infrared Detectors for Astronomy VIII*], *Proc.SPIE* **10709** (2018).
- [24] Hudec, R., “Kirkpatrick-Baez (KB) and Lobster Eye (LE) Optics for Astronomical and Laboratory Applications,” *X-Ray Optics and Instrumentation, 2010. Special Issue on X-Ray Focusing: Techniques and Applications, id.139148* **2010**, 139148 (2010).
- [25] Chattopadhyay, T., Falcone, A., Burrows, D. N., Bray, E., McQuaide, M., Kern, M., Wages, M., Hull, S., Inneman, A., Hudec, R., and Stehlikova, V., “Characterization of X-ray Lobster Optics with a Hybrid CMOS sensor,” in [*American Astronomical Society Meeting Abstracts No. 231*], *American Astronomical Society Meeting Abstracts* **231**, 355.35 (Jan. 2018).
- [26] Chattopadhyay, T., Falcone, A. D., Burrows, D. N., Fox, D. B., and Palmer, D., “Blackcat cubesat: A soft x-ray sky monitor, transient finder, and burst detector for high-energy and multimessenger astrophysics,” in [*Space Telescopes and Instrumentation 2018: Ultraviolet to Gamma Ray*], *Proc.SPIE* **10699** (2018).